# Periostin induces epithelial-to-mesenchymal transition via the integrin α5β1/TWIST-2 axis in cholangiocarcinoma

JUMAPORN SONONGBUA[1], SUCHADA SIRITUNGYONG[1], SUYANEE THONGCHOT[2], THANPAWEE KAMOLHAN[2], KUSUMAWADEE UTISPAN[3], PETI THUWAJIT[2], ANANYA PONGPAIBUL[4], SOPIT WONGKHAM[5,6] and CHANITRA THUWAJIT[2]

[1]Graduate Program in Immunology; [2]Department of Immunology, Faculty of Medicine, Siriraj Hospital, Mahidol University, Bangkok 10700; [3]Faculty of Dentistry, Thammasat University, Pathum Thani 12121; [4]Department of Pathology, Faculty of Medicine, Siriraj Hospital, Mahidol University, Bangkok 10700; [5]Department of Biochemistry; [6]Cholangiocarcinoma Research Institute, Faculty of Medicine, Khon Kaen University, Khon Kaen 40002, Thailand

Received June 18, 2019; Accepted January 21, 2020

DOI: 10.3892/or.2020.7485

**Abstract.** Periostin (PN) (also known as osteoblast-specific factor OSF-2) is a protein that in humans is encoded by the *POSTN* gene and has been correlated with a reduced survival of cholangiocarcinoma (CCA) patients, with the well-known effect of inducing epithelial-to-mesenchymal transition (EMT). The present study investigated the effect of PN, through integrin (ITG)α5β1, in EMT-mediated CCA aggressiveness. The alterations in EMT-related gene and protein expression were investigated by real-time PCR, western blot analysis and zymogram. The effects of PN on migration and the level of TWIST-2 were assessed in CCA cells with and without si*ITGα5* transfection. PN was found to induce CCA cell migration and EMT features, including increments in Twist-related protein 2 (TWIST-2), zinc finger protein SNAI1 (SNAIL-1), α-smooth muscle actin (ASMA), vimentin (VIM) and matrix metallopeptidase 9 (MMP-9), and a reduction in cytokeratin 19 (CK-19) together with cytoplasmic translocation of E-cadherin (CDH-1). Additionally, PN markedly induced MMP-9 activity. *TWIST-2* was significantly induced in PN-treated CCA cells; this effect was attenuated in the ITGα5β1-knockdown cells and corresponded to reduced migration of the cancer cells. These results indicated that PN induced CCA migration through ITGα5β1/TWIST-2-mediated EMT. Moreover, clinical samples from CCA patients showed that higher levels of TWIST-2 were significantly correlated with shorter survival time. In conclusion, the ITGα5β1-mediated TWIST-2 signaling pathway regulates PN-induced EMT in CCA progression, and TWIST-2 is a prognostic marker of poor survival in CCA patients.

## Introduction

Cholangiocarcinoma (CCA) is a primary liver cancer arising from bile duct epithelial cells and characteristically manifests as an abundant stromal reaction (1). CCA is associated with a poor patient prognosis and a low survival rate due to its high capability to invade and metastasize (2). Increased α-smooth muscle actin (ASMA)-positive fibroblasts have been indentified in the stroma of CCA tissues and higher levels have been correlated with shorter patient survival times (1). These fibroblasts were found to have upregulated expression of several secreted proteins, and periostin (PN) is a crucial one exclusively overexpressed in stromal fibroblasts and significantly correlated with poor patient prognosis (3). PN (also known as osteoblast-specific factor OSF-2) is a protein that in humans is encoded by the *POSTN* gene and has been reported to enhance several tumorigenic properties in various types of cancers including ovarian (4), breast (5), colon (6), head and neck (7), and pancreatic cancer (8). Enhancement was shown to occur through interactions with membrane receptor integrin (ITG)αvβ3 or αvβ5 in ovarian cancer (4), ITGα6β4 in pancreatic cancer (9), and ITGα5β1 in CCA (10). Mino *et al* revealed that the malignant potential of PN is expressed through the induction of epithelial-to-mesenchymal transition (EMT) in CCA via ITGαv (11). Although PN acts through ITGα5β1 in CCA cell invasion (10), understanding of the role of ITGα5β1 in the EMT phenotype of CCA cells is still limited.

EMT has been strongly implicated in several types of cancer in regards to a key impact on cell invasion and metastasis (12,13). Characteristics of cells undergoing EMT include an increase in mesenchymal markers such as vimentin (VIM),

*Correspondence to:* Professor Chanitra Thuwajit, Department of Immunology, Faculty of Medicine, Siriraj Hospital, Mahidol University, 2 Prannok Street, Bangkok 10700, Thailand
E-mail: cthuwajit@yahoo.com; chanitra.thu@mahidol.ac.th

*Abbreviations:* CCA, cholangiocarcinoma; EMT, epithelial-to-mesenchymal transition; PN, periostin; ITG, integrin; ASMA, α-smooth muscle actin; VIM, vimentin; MMP, matrix metalloproteinase; CDH-1, E-cadherin; CDH-2, N-cadherin; FN-1, fibronectin; CK, cytokeratin; TGF-β, transforming growth factor-β; TNF-α, tumor necrosis factor-α; HNPCC, head and neck squamous cell cancer; FBS, fetal bovine serum; HGF-α, hepatocyte growth factor α

*Key words:* cholangiocarcinoma, periostin, epithelial-to-mesenchymal transition, TWIST-2, integrin α5β1

N-cadherin (CDH-2), ASMA, and fibronectin (FN-1) and a reduction in epithelial markers, in particular, E-cadherin (CDH-1) and cytokeratin (CK) (14,15). Three transcription factors, zinc finger protein SNAI1 (SNAIL-1), SLUG (SNAIL-2) and TWIST have been demonstrated to function in the regulation of EMT in cancers (14). Zinc finger protein SNAI1 (SNAIL-1) has been identified as a key molecule in transforming growth factor (TGF)-β1-activated EMT in pancreatic cancer (16,17). TWIST was shown to induce breast cancer cells to undergo EMT (18). However, the role of TWIST-2 in EMT that follows PN activation of ITGα5β1 has not been well elucidated. In the present study, recombinant PN activated EMT which led to CCA migration and TWIST-2 activation, and additionally, the potential clinical use of TWIST-2 as a marker for poor prognosis in human CCA was revealed. These findings also highlight the potential impact of targeting the PN/ITGα5β1/TWIST-2 pathway driving CCA migration to attenuate the progression of disease.

## Materials and methods

*CCA cell line culture*. Human CCA cell lines KKU-100, KKU-139 and KKU-213 were cultured in DMEM medium (Invitrogen; Thermo Fisher Scientific, Inc.) supplemented with 10% fetal bovine serum (FBS), 100 U/ml penicillin, 100 $\mu$g/ml streptomycin (Invitrogen; Thermo Fisher Scientific, Inc.), and an anti-fungal agent. Cells were cultured in a 5% $CO_2$ incubator at 37˚C, and passaged with 0.25% trypsin-EDTA. Cells with more than 90% viability were used throughout this study.

*Migration assay (wound healing assay)*. KKU-100, KKU-139, and KKU-213 tumor cell lines (50,000 cells/well) were cultured in 6-well plates until they reached approximately 90% confluence. A reference midline was drawn under the plate. Cells were scraped off along the line using a sterile 200-$\mu$l pipette tip and the detached cells were washed away with serum-free medium. The remaining cells were then treated with medium containing either 100 ng/ml recombinant PN or medium without PN. The scraped area indicated by the reference line was recorded at the beginning of treatment and again at 24 h. The efficiency of migration into the scraped area was taken as a measure of wound healing and was calculated by the following formula: % wound healing=[(wound space at 0 h-wound space at 24 h)/wound space at 0 h] x100.

*Transwell migration assay*. A total of $5x10^4$ KKU-213 cells in DMEM containing 1% FBS with or without 100 ng/ml PN was plated in the upper chamber of a 24-well Corning Transwell plate (Corning #3428 Transwell) and 600 $\mu$l of 1% FBS DMEM was added to the lower chamber. After culture in a humidified incubator at 37˚C for 12 h, the upper chamber was fixed in 70% ethanol for 30 min and stained with 0.5% crystal violet for 15 min. After drying, migrating cells were counted under an inverted microscope (original magnification, x400).

*Measurement of EMT gene expression in PN-treated CCA cell lines by real-time PCR*. Total RNA was extracted using a Perfect Pure RNA Cultured Cell Kit (5 PRIME; Thermo Fisher Scientific, Inc.) according to the manufacturer's instructions. The cDNA was synthesized from 1 $\mu$g of total RNA using SuperScript™ III First-Strand Synthesis System for RT-PCR (M-MLV; Invitrogen; Thermo Fisher Scientific, Inc.) according to the instructions. The sequences of all genes in this study were retrieved from PubMed (www.ncbi.nln.nih.gov) and the primers were designed using Primer 3 software (Version 0.4.0) (Table I). The PCR cycles consisted of: 95˚C for 10 min, followed by 50 cycles of 95˚C for 15 sec and 60˚C (except 58˚C for TWIST-2) for 15 sec. Crossing point data were automatically obtained by the fit-point of Lightcycler® 480 software version 1.5 (https://lifescience.roche.com/en_th/products/lightcycler14301-480-software-version-15.html). *ACTB* (β-actin gene) was used as an internal control. The expression level of each gene in the PN-treated CCA cells was compared to that of the control cells without PN treatment ($2^{-\Delta\Delta Cp}$) as follows (19): $2^{-\Delta\Delta Cp}=2^{-(Cp_{PN}\text{-treated sample-CpACTB})-(Cp\text{untreated control-CpACTB})}$ (To note $C_p$ is the crossing point as calculated by Lightcycler 480 software). The expression of EMT genes in TGF-β-treated cells was used as the positive control for EMT.

*Western blot analysis of EMT markers*. Cells with or without PN treatment were collected after refrigerated centrifugation of the cell suspensions at 400 x g for 5 min. The cell pellets were lysed in 1X sample buffer containing 50 mM Tris-HCl pH 6.8, 2% (w/v) SDS, 10% (v/v) glycerol, 5% (v/v) β-mercaptoethanol and 0.05% (w/v) bromophenol blue. Cell lysates were boiled for 10 min and centrifuged at 8,000 x g for 1 min to remove the undissolved proteins and cell debris. Cell extracts were then separated using 10% SDS-PAGE and transferred onto PVDF membranes (Amersham). The membranes were blocked in 5% skim milk containing TBST for 1 h at room temperature (RT). The immunodetection steps for TWIST-2, ASMA, VIM, CK-19, MMP-9, MMP-13, and ITGα5 were performed using mouse anti-TWIST-2 (dilution 1:250; cat. no. ab57997; Abcam), mouse anti-ASMA (dilution 1:400; cat. no. A5228; Sigma-Aldrich; Merck KGaA), mouse anti-VIM (dilution 1:200; cat. no. sc-6260; Santa Cruz Biotechnology, Inc.), mouse anti-CDH-1 (dilution 1:50; cat. no. sc-71008; Santa Cruz Biotechnology), mouse anti-CK-19 (dilution 1:200; cat. no. sc-6278; Santa Cruz Biotechnology), mouse anti-MMP-9 (dilution 1:100; cat. no. sc-21733; Santa Cruz Biotechnology, Inc.), anti-MMP13 (dilution 1:1,000; cat. no. sc-30073; Santa Cruz Biotechnology, Inc.), and mouse anti-ITGα5 (dilution 1:500, sc-376199; Santa Cruz Biotechnology). The incubation periods of primary antibodies for TWIST-2, ASMA, VIM, CK-19, and ITGα5 were overnight at 4˚C, and those of MMP-9 and MMP-13 were 2 and 1 h, respectively, at RT. The secondary antibodies were HRP-conjugated goat anti-mouse IgG antibody (dilution 1:2,000; cat. no. 62-6620; Zymed, Thermo Fisher Scientific, Inc.) for mouse primary antibody, and HRP-conjugated goat anti-rabbit IgG antibody (dilution 1:3,000; Ab6717; Abcam) for rabbit primary antibody. The immunoreactive signals were visualized by ECL (Thermo Fisher Scientific, Inc.) under Gel Document Syngene (Syngene). The β-actin level was used as an internal control with mouse anti-β-actin (dilution 1:10,000; sc-47778; Santa Cruz). The bands were quantified by ImageJ software (Version 1.52a; National Institutes of Health, Bethesda, MD, USA). The obtained staining intensities of the proteins of interest were then normalized against the intensity of the staining of β-actin protein (ACTB).

Table I. Primer sequences used in the study.

| Gene | Accession no. | Primer (5'-3') | Size (bp) |
|---|---|---|---|
| *MMP-1* | NM_002421 | F: TTCGGGGAGAAGTGATGTTC<br>R: ACCGGACTTCATCTCTGTCG | 156 |
| *MMP-7* | NM_002423 | F: TGTATGGGGAACTGCTGACA<br>R: GAGCATCTCCTCCGAGACCT | 131 |
| *MMP-9* | NM_004994 | F: GCACGACGTCTTCCAGTACC<br>R: TAGCCCACTTGGTCCACCT | 105 |
| *MMP-10* | NM_002425 | F: TGGCCCTCTCTTCCATCATA<br>R: CTGATGGCCCAGAACTCATT | 95 |
| *MMP-13* | NM_002427 | F: GCAGCTGTTCACTTTGAGGA<br>R: CACCAATTCCTGGGAAGTCT | 136 |
| *MMP-14* | NM_004995 | F: GTGGTCTCGGACCATGTCTC<br>R: GGGAGGCAGGTAGCCATATT | 154 |
| *SNAIL-1* | NM_005985 | F: TCTGAGGCCAAGGATCTCCAGGC<br>R: CAGGTTGGAGCGGTCAGCGAA | 243 |
| *SLUG* | NM_003068 | F: AATATGTGAGCCTGGGCGCCCT<br>R: GCTCTGTTGCAGTGAGGGCAAGAA | 163 |
| *TWIST-2* | NM_057179 | F: GCAAGAAGTCGAGCGAAGAT<br>R: CAGCTTGAGCGTCTGGATCT | 221 |
| *CK-19* | NM_002276 | F: AGCTAGAGGTGAAGATCCGCGAC<br>R: GGCATTGTCGATCTGCAGGACAA | 155 |
| *CDH-1* | NM_004360 | F: GCCTGGGACTCCACCTACA<br>R: TCTGAGGCCAGGAGAGGAG | 147 |
| *ASMA* | NM_001613 | F: AGGAAGCAGCTCTATGCTAACAAT<br>R: AACACATAGGTAACGAGTCAGAGC | 379 |
| *FN-1* | NM_054034 | F: GGAAGCCGAGGTTTTAACTGCGAG<br>R: ATGGCAGCGGTTTGCGATGGT | 186 |
| *VIM* | NM_003380 | F: CAGGTGGGACCAGCTAACCAA<br>R: TGCCAGACGCATTGTCA | 152 |
| *ACTB* | NM_001101 | F: CACACTGTGCCCATCTACGA<br>R: CTCCTTAATGTCACGCACGA | 162 |

F, forward; R, reverse. MMP, matrix metalloproteinase; *SNAIL-1*, zinc finger protein SNAI1; *SLUG*, human embryonic protein SNAI2; CK, cytokeratin; *CDH-1*, E-cadherin; *ASMA*, α-smooth muscle actin; *FN-1*, fibronectin; *VIM*, vimentin; *ACTB*, β-actin.

*Zymography*. The conditioned-media of CCA cells that had been treated with PN, or that had been left untreated, were centrifuged at 400 x g for 5 min to remove cell debris, and supernatants were then collected. The supernatants were concentrated with Vivaspin 20 (28932358; GE Healthcare; Merck KGaA) (MWCO 3,000) by centrifugation at 3,750 x g at 4˚C for 2 h. The protein concentrations were measured using the Coomassie Plus Assay Kit (Thermo Fisher Scientific, Inc.). The samples were loaded using 12% SDS-PAGE containing 1 mg/ml gelatin (Ajax Finechem) as a substrate. The electrophoresis was performed at 200 V for 5 min in pre-cooled SDS-PAGE running buffer, followed by prolonged electrophoresis in a 4˚C refrigerator for 1 h 20 min. Afterward, the zymogram gels were twice washed for 30 min with 2.5% Triton X-100 to renature the enzymes. Zymographic activities were processed with developing buffer at 37˚C for 18 h. The results were visualized as clear bands after staining with 0.006% Coomassie blue for 2 h at RT The bands were quantified by ImageJ software. The cut-off at 1.5 for upregulated gene expression was used as it typically causes enough upregulated protein production to affect cell phenotype (3).

*Immunocytochemistry for localization of CDH-1*. KKU-213 and KKU-139 CCA cells (5,000 cells/well) were grown in 96-well plates to 40% confluence and treated with 100 ng/ml PN for 48 h. Cells were washed with 1X PBS pH 7.4 and fixed with 4% paraformaldehyde at RT for 10 min. For cell permeabilization, 0.5% Triton X-100 in 1X PBS was added and incubated at RT for 5 min. The non-specific binding was blocked with 10% (w/v) FBS in 1X PBS with 0.1% triton X-100, and incubated at RT for 1 h. Cells were washed with 1X PBS 3 times and incubated with mouse anti-human CDH-1 antibody (dilution 1:50; cat. no. sc-71008; Santa Cruz Biotechnology, Inc.) overnight at 4˚C. Then, the cells were washed with a blocking solution comprised of 10% (w/v) FBS in 1X PBS with 0.1% Triton X-100, and then incubated with goat anti-mouse

IgG-Cy3 (dilution 1:2,000; cat. no. 115-166-071; Jackson ImmunoResearch). The nuclei were stained with Hoechst at 1:1,000 (Invitrogen Thermo Fisher Scientific, Inc.). After washing, the cells were fixed with 4% paraformaldehyde at RT for 10 min and mounted in 50% glycerol. The positive staining cells were visualized under a fluorescence inverted microscope (Olympus; x400 original magnification). The patterns and localizations (cytoplasmic or nuclear) were recorded.

*Immunofluorescence staining of ITGα5β1.* Cells were plated onto 12-mm glass coverslips in DMEM containing 10% FBS in a 24-well plate at $2x10^4$ cells/well and cultured overnight. Cells were fixed with 4% (w/v) paraformaldehyde for 15 min at RT. The cells were blocked with 1X PBS containing 0.5% BSA for 30 min at RT. The cells were stained with primary antibody, mouse anti-human ITGα5 (dilution 1:100, C-9, Santa Cruz Biotechnology, Inc.), for 2 h at RT in 1X PBS containing 0.5% BSA, and incubated with Cy3-conjugated anti-mouse IgG secondary antibody (dilution 1:2,000; cat. no. 115-166-071; Jackson ImmunoResearch Laboratory Inc.). Based on the fact that the ITGα5 subunit can bind only to the ITGb1 subunit (20), changes in ITGα5 were taken as equivalent to changes in ITGα5β1. The nuclei were stained with Hoechst 33342 (1:1,000; Invitrogen; Thermo Fisher Scientific, Inc.) for 1 h at RT. The stained samples were mounted in 50% glycerol and immunofluorescence images were obtained on an inverted microscope and a confocal microscope (LSM800, Carl Zeiss, Jena, Germany; x63 original magnification).

*Transient knockdown of ITGα5 in CCA cells.* Silencing the expression of ITGα5β1 was performed by transfection with si*ITGα5* (Santa Cruz Biotechnology, Inc.) according to the manufacturer's instructions. Briefly, $1.5x10^5$ cells/well were seeded onto 6-well plates and cultured with complete medium at 37˚C in a 5% $CO_2$ incubator for 24 h. A si*ITGα5* transfection solution was prepared by separately mixing 100 $\mu$l of OptiMEM® I (Invitrogen; Thermo Fisher Scientific, Inc.) with either 10 $\mu$l of 10 pmole si*ITGα5* or 5 $\mu$l of Lipofectamine™ 2000 (Invitrogen; Thermo Fisher Scientific, Inc.). The solutions were then mixed and incubated for 20 min at RT. In addition, 200 $\mu$l of OptiMEM® I mixed with 5 $\mu$l of Lipofectamine™ 2000 was simultaneously used as a mock solution. Cells were washed three times with antibiotic-serum-free medium. The si*ITGα5* transfection solution (cat. no. STCSC-29372, Santa Cruz Biotechnology, Inc.) was slowly dropped into each well and incubated at 37˚C in a 5% $CO_2$ incubator for 6 h. Then the complete medium was replaced. The efficiency of ITGα5 silencing was confirmed by real-time PCR and immunofluorescence staining.

*Immunohistochemistry of ITGα5β1 and TWIST-2 in CCA tissues.* Paraffin-embedded tissue samples from 50 CCA cases were collected from the Cholangiocarcinoma Research Institute, Faculty of Medicine, Khon Kaen University (Khon Kaen, Thailand) under the approval of the Human Research Ethics Committee, Khon Kaen University (HE490143). The median age of the patients was 58 years with a range of 37-75 years. The percentage of females was 38% (19/50) and males was 62% (31/50). The samples were recruited during 2006-2011. The tissues were baked at 60-65˚C for 4 h, deparaffinized, soaked in 10 mM citrate buffer pH 6, and boiled at 95˚C for 40 min. Endogenous peroxidase was blocked with 3% $H_2O_2$ in methanol for 30 min. The tissues were incubated with 2% BSA in 0.05 M Tris-HCl pH 7.6 to block non-specific binding, then mouse anti-human TWIST-2 (dilution 1:200; ab57997; Abcam) was applied and the tissues were incubated at 4ºC overnight. The tissues were then incubated with EnVision+ System horseradish peroxidase (Dako) for 30 min. The signal was developed using 0.05% 3,3'-diaminobenzidine (DAB) and counterstained with hematoxylin. The scoring was assessed using the percentage of positive staining cells (P) and the intensity of the staining signal (I). For P, samples containing 0-25, 26-50, 51-75, and 76-100% positive cells were classified as grades 0, 1, 2, and 3, respectively. For I, unstained, slightly stained, intermediately stained, and strongly stained cells were classified as 0, 1, 2, and 3, respectively. The multiplied score (P x I) as a total score of 0-9 was determined for each stained slide by 2 investigators double-blinded to the clinical data. A total score of more than 4 was classified as high TWIST-2 level whereas scores less than or equal to 4 were in the low-level group. This cut-off value was derived from the median of the scoring of all cases. In this research study, the normal adjacent area which was approximately 5-10 mm distant from the border of the cancerous area in the same slide of the CCA tissue section was used to represent normal bile duct.

For ITG*α5β1*, the level in CCA tissues was detected using the same protocols as for TWIST-2 except that the antigen retrieval was performed using samples microwave-heated with 10 mM sodium citrate buffer with 0.05% Tween 20, pH 6.0 for 10 min, and the mouse anti-human ITG*α5* antibody (dilution 1:100, sc-376199; Santa Cruz Biotechnology, Inc.) was used as the primary antibody.

*Statistical analysis.* All quantified data are expressed as mean ± standard deviation (SD), except for survival time for which median values were used. Statistics for the *in vitro* studies were compared with controls using the Student's t-test. One-way analysis of variance (ANOVA) with all pairwise multiple comparison by Tukey test was utilized to analyze the significant results of more than 2 groups. The statistical analysis of two variables and the interaction between the groups was performed by two-way ANOVA. The correlation of TWIST-2 level with clinicopathological data was verified by Cox regression multivariate analysis, and the Kaplan-Meier Log Rank test was used for survival analysis. A P-value of $<0.05$ was considered to be statistically significant.

## Results

*PN-induced alterations in the EMT phenotype and EMT-related markers in CCA cells.* The results revealed with statistical significance that KKU-213 CCA cells treated with 100 ng/ml PN had a greater ability to migrate than the untreated control cells, which had a migration ability similar to CCA cells treated with 10 ng/ml TGF-β (Fig. S1). Upregulated genes in the PN-treated cells were defined as those with relative gene expression 1.2-fold over those in the untreated cells. Downregulated genes had a relative gene expression equal to or less than 0.8-fold. The results showed

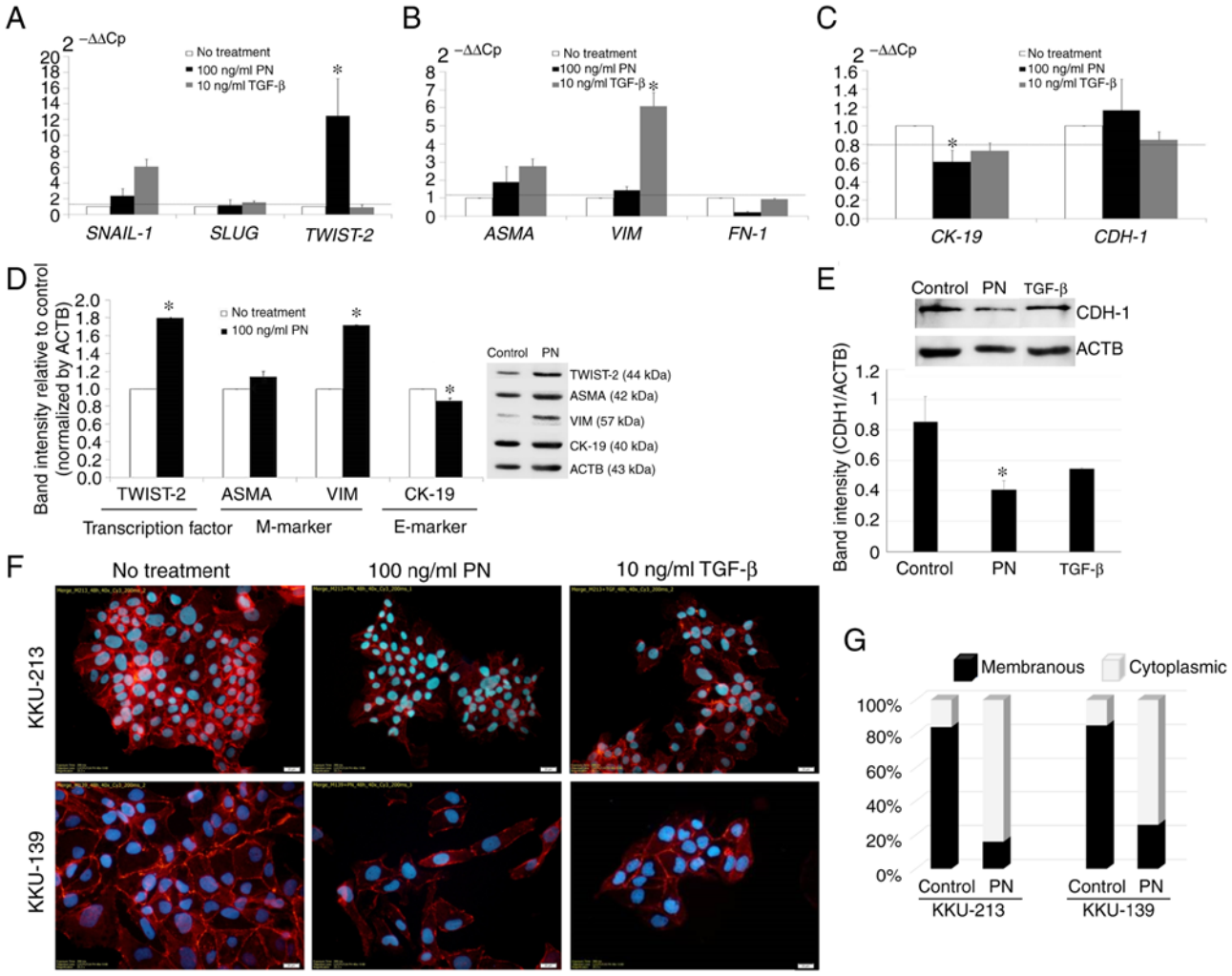


Figure 1. PN-induced alterations in EMT-related genes. (A-C) Real-time PCR analysis of mRNA in KKU-213 CCA cells was conducted after treatment with 100 ng/ml PN. Gene expression in excess of 1.2 times that of the negative control, (i.e. above the dashed line), was scored as upregulation. (A) EMT-regulated transcription factors. (B) Mesenchymal markers. (C) Epithelial markers. Cells cultured in serum-free media without PN were used as the negative control. Results are represented as mean ± SD of triplicate reactions in one to three independent experiments. *P<0.05 compared to the untreated control which was assumed to be one. (D) Western blot analysis of TWIST-2, ASMA, VIM, and CK-19. Band intensity of EMT markers quantified by ImageJ software was determined relative to the control without PN treatment, and normalized by ACTB. The bars represent the mean ± SD of two measurements. (E) The alteration of CDH-1 after PN treatment compared to ACTB. (F) Immunocytochemical localization of CDH-1 in CCA cell lines induced by PN. TGF-β was used as an EMT stimulant. Original magnification, x400 (scale bar, 20 mm). (G) Bar graphs representing the distribution of CDH-1 staining in CCA cells with and without PN treatment. PN, periostin; EMT, epithelial-to-mesenchymal transition; CCA, cholangiocarcinoma; TWIST-2, Twist-related protein 2; ASMA, α-smooth muscle actin; VIM, vimentin; MMP, matrix metalloproteinase; CK, cytokeratin; *ACTB*, β-actin; CDH-1, E-cadherin; FN-1, fibronectin; TGF-β, transforming growth factor-β; *SNAIL-1*, zinc finger protein SNAI1; *SLUG*, human embryonic protein SNAI2.

that PN treatment induced the expression of both *SNAIL-1* and *TWIST-2*, with statistical significance only for *TWIST-2* (Fig. 1A). Notably, *SNAIL-1* was activated by both PN and TGF-β, whereas *SLUG* was not changed. Upregulation of *ASMA* and *VIM* mesenchymal markers was observed in the PN-treated CCA cells (Fig. 1B). Downregulation of the *CK-19* epithelial marker was significant, whereas no significant change was observed in the *CDH-1* mRNA level (Fig. 1C). The Western blot results confirmed that the PN-induced EMT of CCA cells was accompanied by significant downregulation of *CK-19*, and a significant increase in the production of TWIST-2 and VIM (Fig. 1D).

Interestingly, although the difference in the expression level of *CDH-1* mRNA was not significant, the protein level revealed by western blot analysis was significantly reduced in the PN-treated cancer cells (Fig. 1E). This was supported by the finding in TGF-β-treated cells. Moreover, CDH-1, expressed predominantly on the cell membranes of both KKU-213 and KKU-139 CCA cells, was translocated after PN treatment to the cytoplasm (Fig. 1F). Thus, the membrane localization of CDH-1 in the untreated cells was found on approximately 84 and 85% of the KKU-213 and KKU-139 cells (Fig. 1G). In cells treated with PN, the membranous protein staining pattern of CDH-1 was reduced to 16 and 26% of KKU-213 and KKU-139 cells respectively, and the percentages of cells displaying a cytoplasmic staining pattern was increased to approximately 84 and 74%.

*Effect of PN on the induction of MMPs in CCA cells*. No alterations of *MMP-1*, *MMP-7*, *MMP-10*, or *MMP-14* were detected in PN-treated CCA cells, whereas 100 ng/ml PN induced levels of *MMP-9* and *MMP-13* to 1.99±0.21- and

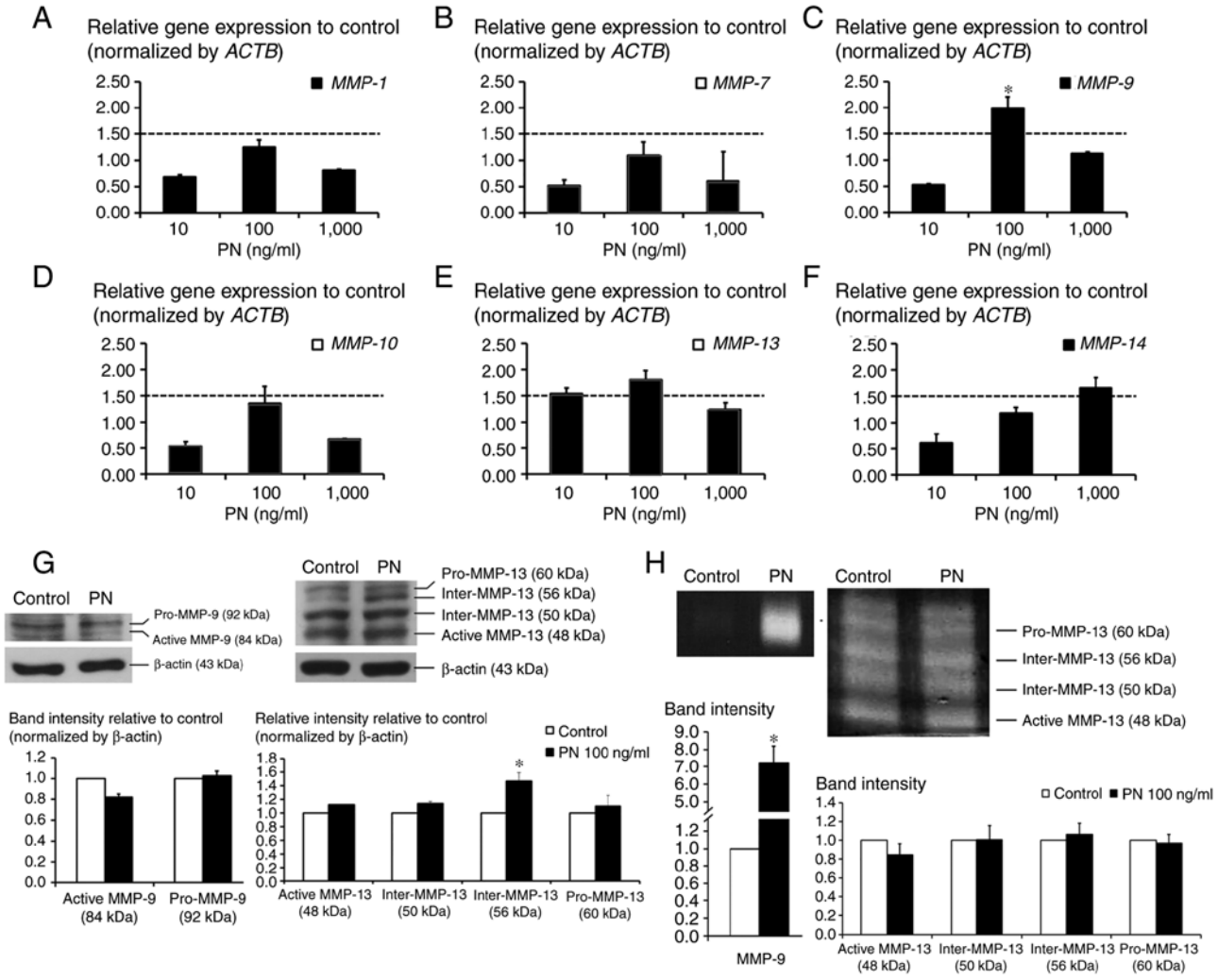


Figure 2. Levels of MMPs in PN-treated KKU-213 CCA cells. (A-F) Cells were treated with 10-1,000 ng/ml PN before analysis of *MMP* expression by real-time PCR. Relative gene expression of PN-treated cells compared to a control without PN that was >1.5 was specified as upregulated. Results are presented as mean ± SD of duplicate PCR reactions in two independent experiments. (G) Western blot analysis of MMP-9 and MMP-13 in PN-treated CCA cells compared with a control without PN treatment. Equal loading was confirmed by β-actin. (H) The proteolytic activities of MMP-9 and MMP-13 in PN-treated CCA cells. Band intensities of each MMP were quantified by ImageJ software and compared to the controls without PN treatment. Bars represent means ± SD of two measurements. *P<0.05 of PN-treated cells compared to that in untreated cells. MMPs, matrix metalloproteinases; PN, periostin; CCA, cholangiocarcinoma; Inter-MMP, intermediate form of MMP; *ACTB*, β-actin.

1.81±0.17-fold that of the untreated control cells (Fig. 2A-F). However, the western blot analysis results showed that neither pro-MMP-9 (92 kDa) nor active MMP-9 (84 kDa) were induced by PN whereas the intermediate form of MMP-13 (Inter-MMP-13) at 56 kDa showed a significant increase (Fig. 2G). The zymography results showed that after exposure to PN, CCA cells secreted MMP-9 into the conditioned-medium with a marked increase in activity compared to the activity observed in the control condition (Fig. 2H). Densitometric analysis showed that MMP-9 activity was significantly increased in the PN-treated CCA cells to 7-fold that of the control cells. No significant change in MMP-13 in the PN-treated CCA cells was observed.

*ITGα5β1-mediated CCA cell migration and MMP expression*. The si*ITG5*-transfection significantly downregulated intrinsic *ITG5* mRNA expression with an efficiency of approximately 35-50% (Fig. 3A). The efficiency of knockdown was significant in cells up to 96 h post-siRNA treatment (Fig. 3B). The wound-closure assay showed that PN significantly induced CCA cell migration after 24 h of treatment, while in the si*ITGα5*-transfected cells, the migration was slower than that in the mock-transfected cells (Fig. 3C). In cells in which ITGα5β1 was diminished, the induction of expression of both *MMP-9* and *MMP-13* by PN treatment was less than that in the mock-transfected cells. This difference was significant for MMP-9 (Fig. 3D and E).

*ITGα5β1/TWIST2-mediated CCA cell migration*. The results showed that si*ITGα5* treatment successfully inhibited the production of membrane ITGα5β1 in CCA cell lines (Fig. 4A). Moreover, the si*ITGα5*-transfected cells had a significantly lower response rate in the PN-induced cell migration assay compared to the scrambled-siRNA-treated cells (Fig. 4B). These results were observed in all three CCA cell lines. TWIST-2 levels in these *ITGα5*-transient-knockdown CCA cells were not induced by PN and this was in accord with the decreased level of cell migration induced by PN (Fig. 4C).

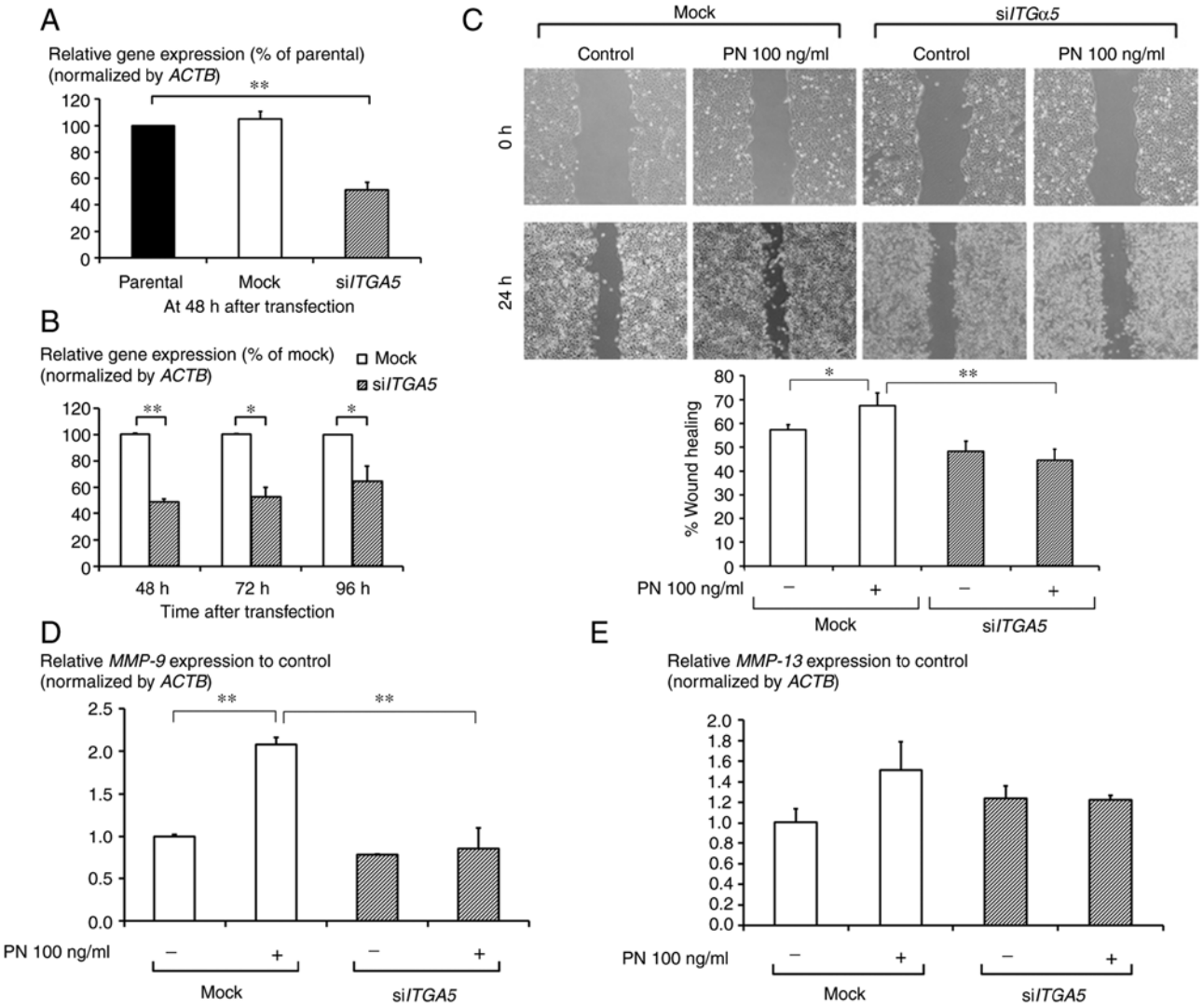


Figure 3. Transient *ITGα5* knockdown in KKU-213 CCA cells and the responses to PN. (A) si*ITGα5* transfection (si*ITGα5)* achieved efficient knockdown of *ITGα5* expression. (B) Knockdown of *ITGα5* expression was observed from 48 to 96 h after transfection. (C) Comparison of wound healing between intrinsic *ITGα5*-expressing and *ITGα5*-silenced cells after treatment with PN is shown. The wound closure areas were visualized under an inverted microscope with a magnification of x40. (D and E) Expression of *MMP-9* and *MMP-13* after PN treatment of intrinsic *ITGα5*-expressing and *ITGα5*-silencing cells. β-actin gene (*ACTB*) was used as an internal control. Bar graphs show mean ± SD of independent experiments. $^{*}$P<0.05, $^{**}$P<0.01. ITG, integrin; CCA, cholangiocarcinoma; PN, periostin; MMP, matrix metalloproteinase.

*Expression of ITGα5β1 and TWIST-2 in CCA tissues and the clinicopathological relevance*. The demographic data of the enrolled patients are shown in Table II. Most of the cases (60%) were male and more than 90% of the enrolled cases were diagnosed with late-stage disease. Various positive stain-intensity scores of TWIST-2 were found in CCA tissues (Fig. 5A-C) whereas normal bile duct showed no TWIST-2 expression (Fig. 5D). Most of the CCA cases, (33/50, 66%), showed high TWIST-2 levels. Multivariate Cox regression analysis revealed that elevated TWIST-2 level and a categorization as a poorly differentiated cancer type were independent parameters associated with poor prognosis. Other parameters showed no significant correlations. Interestingly, CCA patients with high TWIST-2 had shorter mean survival times (211±14 days) compared to those with low TWIST-2 (637±503 days). The overall survival analysis by Kaplan-Meier test showed, with statistical significance, that patients exhibiting high TWIST-2 levels had shorter survival times than those with low TWIST-2 using both 3-year and 5-year survival as the cut-off values (Fig. 5E). The level of ITGα5β1 in CCA clinical samples was also explored, and the results showed elevated expression in 70% (7/10) of the CCA cases. The levels ranged from low to high expression (Fig. 5F).

## Discussion

Epithelial-to-mesenchymal transition (EMT) is a transient phenomenon but is an important step in cancer cell activation by many intracellular and extracellular stimuli, including soluble substances from both cancer cells and cancer stromal fibroblasts in the cholangiocarcinoma (CCA) microenvironment (21-23). The aberration of secretomes in ASMA-positive stromal fibroblasts led to the discovery of periostin (PN) as a major protein having a tumorigenic impact in intrahepatic CCA (3), and a variety of EMT markers have been proposed as indicators for the poor

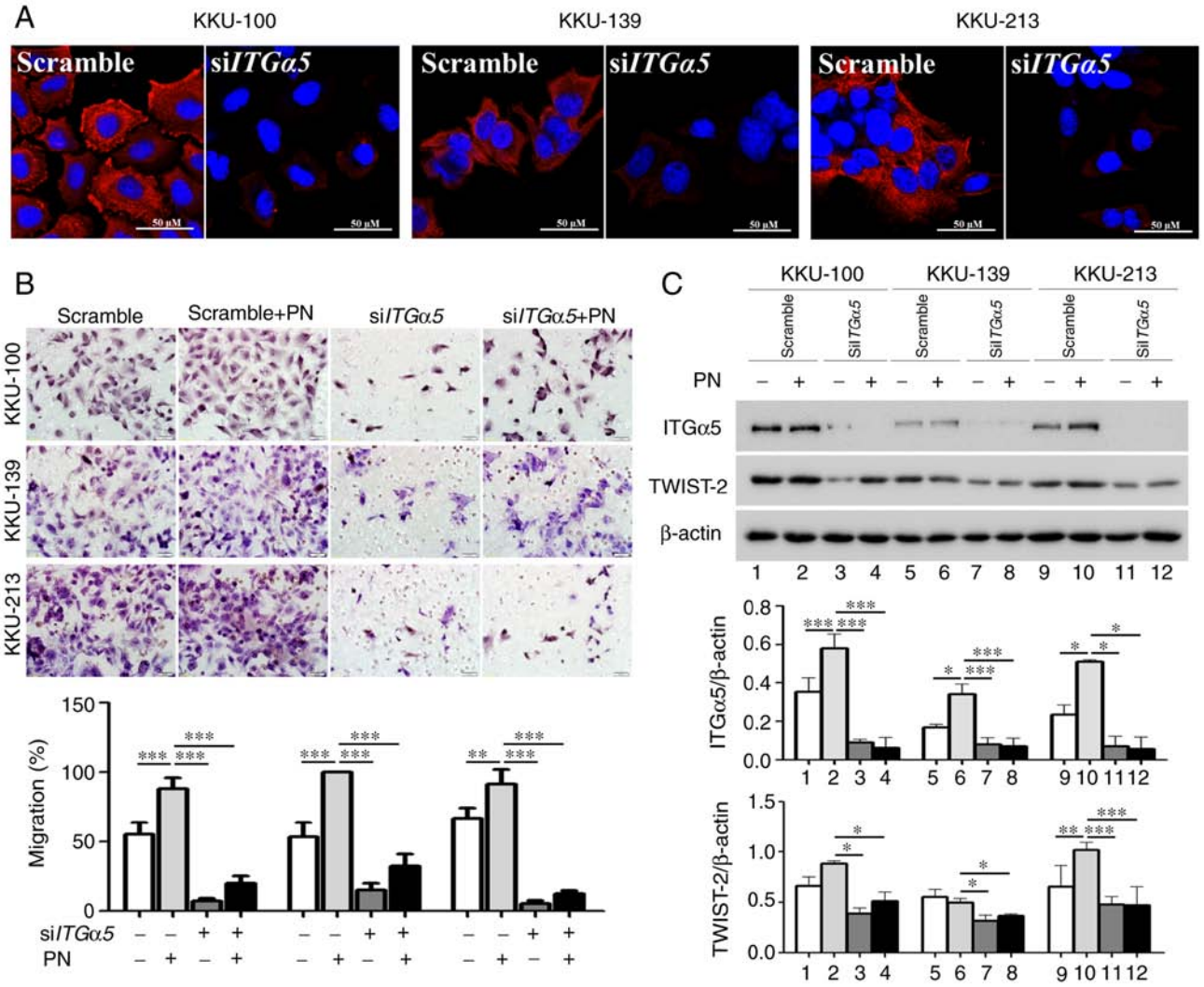


Figure 4. Effect of transient *ITGα5* knockdown (si*ITGα5)* on the migration response of CCA cells to PN. (A) Downregulation of ITGα5 in si*ITGα5*-treated CCA cells detected by immunocytochemistry as determined by confocal microscopy. Original magnification, x63. Scale bar, 50 mm. (B) Significant migration ability of CCA cells after treatment with PN compared to the absence of response in si*ITGα5*-treated CCA cells. (C) Increased level of TWIST-2 after PN treatment in ITGα5-expressing CCA cells and attenuated response in the cells with suppressed expression of ITGα5. Results are presented as mean ± SD of triplicate experiments. $^{*}$P<0.05, $^{**}$P<0.01 and $^{***}$P<0.001. ITG, integrin; CCA, cholangiocarcinoma; PN, periostin; TWIST-2, Twist-related protein 2.

patient prognosis (24). The present study confirms the effect of PN on the EMT phenotype in CCA cells and is consistent with recently published research indicating that this protein acts in an autocrine manner (11).

The high level of ITGα5β1 in CCA cell lines and its role as a receptor for PN have been reported in our previous publication (10). In the present study, it was revealed that PN treatment of CCA cell lines induced an EMT pattern of gene expression that included upregulation of ASMA and VIM, an increase in MMP-9 activity, and downregulation of CK-19 through the ITGα5β1 and TWIST-2 signaling pathway. Additionally, the level of TWIST-2 was correlated with patient survival time, with statistical significance. These findings highlight the potential impact of inhibiting the PN/ITGα5β1/TWIST-2-pathway that drives CCA migration, thereby attenuating the progression of this disease.

The expression pattern of EMT markers in PN-induced CCA cell lines revealed alterations and translocation of membranous CDH-1 to the cytoplasm of cells. This hallmark of EMT gene expression has also been found in TNF-α and HGF-α-treated CCA cells (21,23). Although *CDH1* mRNA in periostin-treated cells was not significantly changed compared to the control untreated cells, the protein level was reduced. The level of protein, the final product, is considered to be more relevant than the mRNA level. Moreover, there is an evident showing that PN regulated EMT and EMT transcriptional factor expression by repressing microRNA-38 expression in lung cancer (25). In the same way, CDH-1 was shown in breast cancer to be downregulated by miR-9 resulting in increased cell motility and invasiveness (26). These findings highlight the potential of PN to regulate gene expression at the post-transcriptional or translational level which supports the finding of unaltered mRNA but an altered protein level of CDH-1 in the study herein. Cells need membranous CDH-1 to provide intercellular molecular adhesion and attachment to extracellular matrices (27) and a decrease in membranous CDH-1 in PN-treated CCA cells facilitates subsequent cell detachment and migration. The level of CK-19 was also reduced by PN, as previously reported in cells treated with TGF-β and TNF-α (22,23). Evidently,

Table II. TWIST-2 covariates to the survival of CCA patients in the multivariate Cox regression analysis.

| | 3-year survival | | | 5-year survival | | |
|---|---|---|---|---|---|---|
| Variable (n=50) | Hazard ratio | 95% CI | P-value | Hazard ratio | 95% CI | P-value |
| TWIST-2 level | | | 0.022[a] | | | 0.023[a] |
| Low (n=17) | 2.687 | 1.153-6.259 | | 2.485 | 1.135-5.439 | |
| High (n=33) | | | | | | |
| Age, in years | | | 0.338 | | | 0.281 |
| ≤57 (n=24) | 1.405 | 0.701-2.816 | | 1.458 | 0.734-2.893 | |
| >57 (n=26) | | | | | | |
| Sex | | | 0.219 | | | 0.414 |
| Male (n=32) | 0.643 | 0.319-1.299 | | 0.759 | 0.392-1.470 | |
| Female (n=18) | | | | | | |
| Histological type | | | | | | |
| WD (n=21) | 1.000 | | | 1.000 | | |
| MD (n=8) | 1.336 | 0.563-3.170 | 0.511 | 1.186 | 0.510-2.759 | 0.692 |
| PD (n=6) | 4.670 | 1.648-13.24 | 0.004[a] | 4.466 | 1.617-12.33 | 0.004[a] |
| Pap (n=15) | 2.070 | 0.681-6.292 | 0.199 | 2.158 | 0.772-6.032 | 0.143 |
| Vascular invasion | | | 0.878 | | | |
| Presence (n=8) | 1.071 | 0.444-2.582 | | 0.900 | 0.380-2.129 | 0.900 |
| Absence (n=42) | | | | | | |
| Stage | | | 0.450 | | | |
| I-II (n=4) | 1.1763 | 0.404-7.668 | | 1.247 | 0.369-4.215 | 0.723 |
| III-IV (n=46) | | | | | | |
| Tumor size (cm) | | | 0.713 | | | |
| ≤5 (n=27) | 1.147 | 0.553-2.378 | | 1.185 | 0.581-2.417 | 0.641 |
| >5 (n=23) | | | | | | |

[a]P<0.05 indicates significant difference. CCA, cholangiocarcinoma; TWIST-2, Twist-related protein 2; CI, confidence interval; WD, well-differentiated; MD, moderately differentiated; PD, poorly differentiated; Pap, papillary.

the PN-induced EMT phenomenon in CCA cells displays the characteristic decrease in CK-19 and cytoplasmic translocation of CDH-1, which are important steps allowing cells to detach and become ready to move. The reduction in the CK level is an important characteristic of EMT in CCA (24) and is associated with neural invasion, intrahepatic metastasis, and shortened overall survival time of patients (28). Hence, the lower CK-19 level in PN-treated cells than that noted in the untreated controls represents the induction of EMT in PN-treated CCA cells. To accomplish cell motility, cytoskeletal proteins must increase their expression. In CCA cells activated by PN, the expression levels of *ASMA* and *VIM* were found to be increased which is consistent with increased motility through ASMA-mediated cell-generated mechanical tension, cytoskeleton remodeling (29) and VIM-regulated cell adhesion and migration (30). VIM appears to be a consistent characteristic of EMT in CCA as it was observed both using TGF-β1 as the positive control EMT inducer (22), and using PN as presented in this present study. Interestingly, PN-treated CCA cells that have undergone EMT in highly confluent cultures were found to exhibit epithelial cell morphology (cobblestone shape) while spindle-shaped cells were observed in areas with low confluence, which is consistent with previous findings (31). Serum MMP-9 has been reported as being increased in CCA patients (32) and high expression of tissue MMP-9 has been correlated with poor patient prognosis (33). Herein, PN-stimulated CCA cells had increased levels of MMP-9 and this alteration may help CCA cells to invade through the degraded extracellular matrix consequently leading to distant metastases. PN-induced MMP expression was observed to display a dose-dependent trend in the range of 10-100 ng/ml, for which 1,000 ng/ml was an excessive level, and a feedback inhibition effect is expected (3). We previously showed that ITGα5β1 is the major receptor for PN on the CCA cell membrane (10). The involvement of ITGα5β1 in the regulation of the PN-activated EMT pathway was confirmed here by the finding that cells silenced for ITGα5β1 had both less migration ability induced by PN treatment and reduced MMP production.

SNAIL-1 has been postulated to control the EMT phenotype in CCA cells after stimulation with TGF-β1 and TNF-α (22,23). In a similar way to these previous findings, the present study showed that PN-treated CCA cells

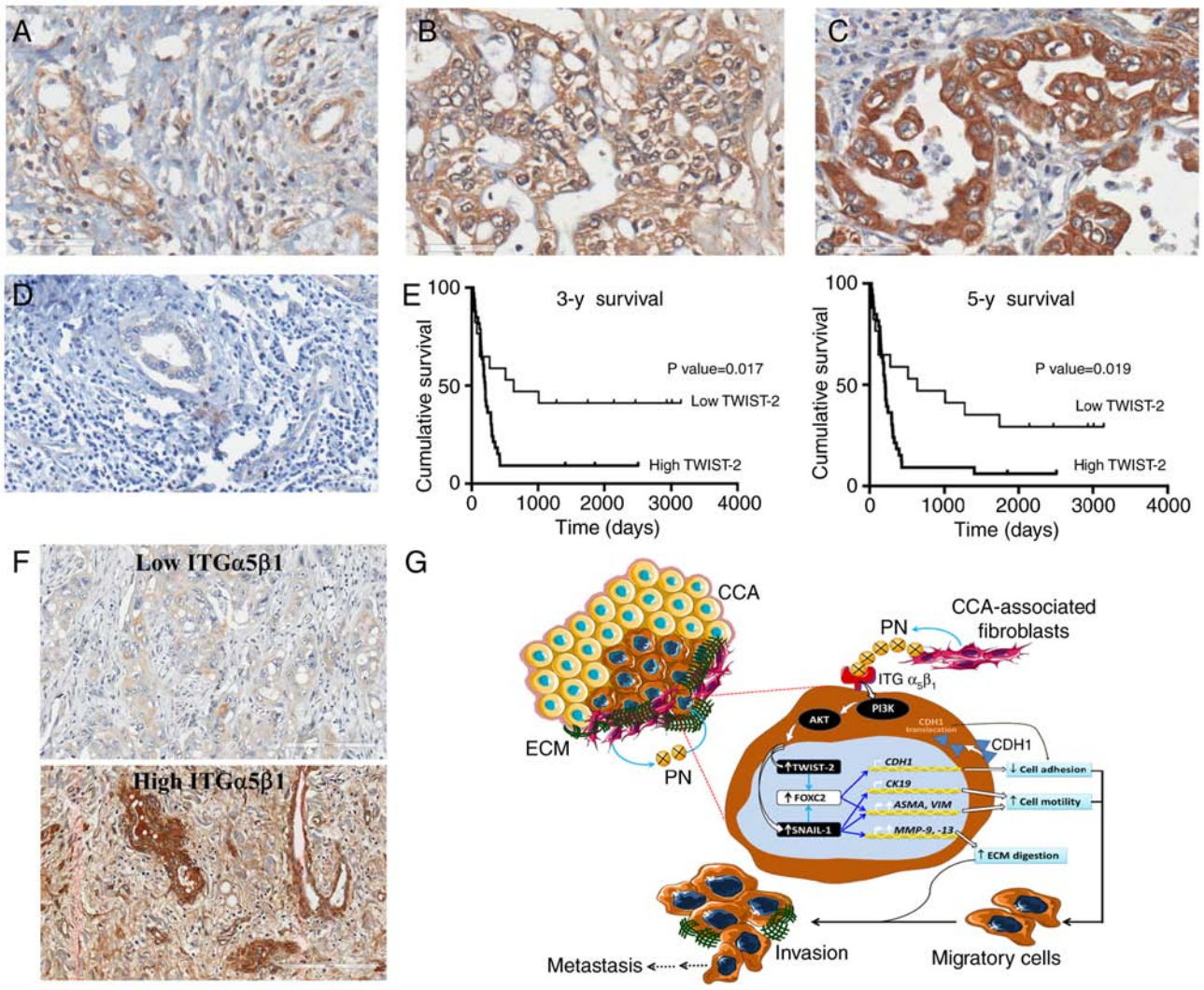


Figure 5. Immunohistochemical staining of TWIST-2 and ITGα5β1 in CCA tissues. (A-D) Representative images showing the stain intensity range. A, grade 1; B, grade 2; C, grade 3; D, no staining in a normal bile duct (original magnification x400; scale bar, 50 $\mu$m). (E) Kaplan-Meier analysis of the 3-year and 5-year survival of patients with high and low TWIST-2 levels. (F) Representative images of low and high expression of ITGα5 in CCA (original magnification x200; scale bar, 200 $\mu$m). (G) Proposed mechanism of PN-induced EMT in CCA. The PN-mediated PI3K-dependent pathway leads to the increased level of TWIST-2 and SNAIL-1, facilitating: i) The reduction in membranous CDH-1 and CK-19 causing loss of cell-to-cell adhesio; ii) decreased levels of ASMA and VIM causing cell motility, and iii) increased levels of MMPs causing ECM degradation. TWIST-2, Twist-related protein 2; ITG, integrin; CCA, cholangiocarcinoma; PN, periostin; EMT, epithelial-to-mesenchymal transition; SNAIL-1. zinc finger protein SNAI1; CDH-1, E-cadherin; CK-19, cytokeratin 19; ASMA, α-smooth muscle actin; VIM, vimentin; MMPs, matrix metalloproteinases; ECM, extracellular matrix.

exhibited increments of *SNAIL-1* and *TWIST-2* mRNA. Increased SNAIL-1 and TWIST-2 proteins were also found and the increase in TWIST-2 was statistically significant. This may imply an involvement of TWIST-2 in PN-induced EMT in CCA cells, particularly as cells with suppressed *ITGα5β1* had a decreased capability to activate TWIST-2 and this corresponded to a decreased ability of the cells to migrate. TWIST-2 has been shown to control the membrane translocation of CDH-1 through FOXC-2 activation (34) which mediates several EMT phenotypes including those of detached and motile cells (35). This function of TWIST-2 was supported by a finding in cervical cancer cell lines demonstrating that lower intrinsic expression of cytoplasmic CDH-1 was exhibited in cells with high TWIST-2 levels (36). In addition, SNAIL-1 was found to play an important role in CCA activation by PN, probably through the downregulation of CK-19 and upregulation of ASMA, VIM, and MMPs (22,23). Herein, it was evident that TWIST-2 may have had a strong impact after activation via the PN/ITGα5β1 pathway in EMT-mediated CCA progression. However, *TWIST-2* overexpression should be carried out in *ITGα5*-knockdown cells to rescue the cell response to PN to further validate TWIST-2 in regards to the effects of PN through ITGα5β1 on CCA cells.

Increased expression of *TWIST-2* has been associated with metastases in the progression of breast and cervical cancers, and is also correlated with poor cell differentiation and a short patient survival rate (36,37). This is similar to the findings of the present study; those patients with high levels of TWIST-2 had significantly shorter survival times compared to those with low TWIST-2. Increases in the SNAIL-1 level in CCA tissues were previously reported to significantly correlated with lymph node metastasis and a poor survival rate in CCA patients (22). This is in contrast to the findings with extrahepatic CCA, in

which SNAIL, SLUG, TWIST, ZEB1, ZEB2 were not valuable to predict poor outcomes of the patients, whereas VIM, FN, S100A4, CDH1, and CDH2 were associated with short survival times (38).

In conclusion, PN enrichment found in the CCA microenvironment, mainly produced by cancer-associated fibroblasts, activates CCA cells by binding to ITGα5β1 to trigger an AKT-dependent signaling pathway (10) that activates TWIST-2 (Fig. 5G). Although the limitation of FOXC2 was not identified, this study identified alterations in EMT-related genes underlying changes in the phenotype for EMT and driving CCA progression after the binding of PN to ITGα5β1. The change in TWIST-2 levels can be suggested as a marker of poor prognosis that predicts the aggressiveness of CCA. Moreover, clinically targeting this ITGα5β1-mediated pathway and the activated signaling molecules and/or associated transcription factors may help attenuate PN-induced CCA progression.

**Acknowledgements**

We thank Dr Jan Davies of Mahidol University for assisting with the English editing of the manuscript.

**Funding**

This research project was co-supported by MAG Window II, TRF (MRG-WII525S084) and the Faculty of Medicine of Siriraj Hospital. JS was supported by the Development and Promotion of Science and Technology Talents Project (DPST). ST and TK are research assistants supported by the Research Division, Faculty of Medicine, Siriraj Hospital, Mahidol University.

**Availability of data and material**

The datasets used and/or analyzed during the present study are available from the corresponding author on reasonable request.

**Authors' contributions**

JS, SS, KU, ST and CT designed the experiments; JS, SS, ST, TK and KU performed the main research work. AP and SW prepared the samples in preparation for the experiments and facilitated the research work. PT and CT discussed and analyzed the data and results. CT reviewed the paper for research grant application, prepared figures, wrote, and improved the scientific quality of the manuscript, and finally submitted the manuscript. All authors read and approved the manuscript and agree to be accountable for all aspects of the research in ensuring that the accuracy or integrity of any part of the work are appropriately investigated and resolved.

**Ethics approval and consent to participate**

Fifty cases of CCA tissues were obtained from patients who had undergone hepatectomy using the protocol approved by the Human Research Ethics Committee, Khon Kaen University (HE490143). Each patient was informed and written informed consent was obtained.

**Patient consent for publication**

Not applicable.

**Competing interests**

The authors declare that there are no competing interests.

**Authors' information**

JS and SS were enrolled in the Graduate Program in Immunology, Department of Immunology, Faculty of Medicine, Siriraj Hospital, Mahidol University. ST and TK are research assistants under the Research Unit, Faculty of Medicine, Siriraj Hospital, Mahidol University.

**References**

1. Chuaysri C, Thuwajit P, Paupairoj A, Chau-In S, Suthiphongchai T and Thuwajit C: Alpha-smooth muscle actin-positive fibroblasts promote biliary cell proliferation and correlate with poor survival in cholangiocarcinoma. Oncol Rep 21: 957-969, 2009.
2. Nakagohri T, Kinoshita T, Konishi M, Takahashi S and Gotohda N: Surgical outcome and prognostic factors in intrahepatic cholangiocarcinoma. World J Surg 32: 2675-2680, 2008.
3. Utispan K, Thuwajit P, Abiko Y, Charngkaew K, Paupairoj A, Chau-in S and Thuwajit C: Gene expression profiling of cholangiocarcinoma-derived fibroblast reveals alterations related to tumor progression and indicates periostin as a poor prognostic marker. Mol Cancer 9: 13, 2010.
4. Gillan L, Matei D, Fishman DA, Gerbin CS, Karlan BY and Chang DD: Periostin secreted by epithelial ovarian carcinoma is a ligand for alpha(V)beta(3) and alpha(V)beta(5) integrins and promotes cell motility. Cancer Res 62: 5358-5364, 2002.
5. Puglisi F, Puppin C, Pegolo E, Andreetta C, Pascoletti G, D'Aurizio F, Pandolfi M, Fasola G, Piga A, Damante G and Di Loreto C: Expression of periostin in human breast cancer. J Clin Pathol 61: 494-498, 2008.
6. Bao S, Ouyang G, Bai X, Huang Z, Ma C, Liu M, Shao R, Anderson RM, Rich JN and Wang XF: Periostin potently promotes metastatic growth of colon cancer by augmenting cell survival via the Akt/PKB pathway. Cancer Cell 5: 329-339, 2004.
7. Kudo Y, Ogawa I, Kitajima S, Kitagawa M, Kawai H, Gaffney PM, Miyauchi M and Takata T: Periostin promotes invasion and anchorage-independent growth in the metastatic process of head and neck cancer. Cancer Res 66: 6928-6935, 2006.
8. Baril P, Gangeswaran R, Mahon PC, Caulee K, Kocher HM, Harada T, Zhu M, Kalthoff H, Crnogorac-Jurcevic T and Lemoine NR: Periostin promotes invasiveness and resistance of pancreatic cancer cells to hypoxia-induced cell death: Role of the beta4 integrin and the PI3k pathway. Oncogene 26: 2082-2094, 2007.
9. Ben QW, Jin XL, Liu J, Cai X, Yuan F and Yuan YZ: Periostin, a matrix specific protein, is associated with proliferation and invasion of pancreatic cancer. Oncol Rep 25: 709-716, 2011.
10. Utispan K, Sonongbua J, Thuwajit P, Chau-In S, Pairojkul C, Wongkham S and Thuwajit C: Periostin activates integrin α5β1 through a PI3K/AKT-dependent pathway in invasion of cholangiocarcinoma. Int J Oncol 41: 1110-1118, 2012.
11. Mino M, Kanno K, Okimoto K, Sugiyama A, Kishikawa N, Kobayashi T, Ono J, Izuhara K, Kobayashi T, Ohigashi T, *et al*: Periostin promotes malignant potential by induction of epithelial-mesenchymal transition in intrahepatic cholangiocarcinoma. Hepatol Commun 1: 1099-1109, 2017.
12. Cervantes-Arias A, Pang LY and Argyle DJ: Epithelial-mesenchymal transition as a fundamental mechanism underlying the cancer phenotype. Vet Comp Oncol 11: 169-184, 2013.
13. Xu W, Yang Z and Lu N: A new role for the PI3K/Akt signaling pathway in the epithelial-mesenchymal transition. Cell Adhes Migr 9: 317-324, 2015.
14. Son H and Moon A: Epithelial-mesenchymal transition and cell invasion. Toxicol Res 26: 245-252, 2010.
15. Tsai JH and Yang J: Epithelial-mesenchymal plasticity in carcinoma metastasis. Genes Dev 27: 2192-2206, 2013.

16. Song L, Wang P, Tian Y, Chang D, Li K, Fan Y, Shen J, Du H, Mi R, Bian X and Tang X: Lung metastasis of pancreatic carcinoma is regulated by TGFβ signaling. Tumour Biol 36: 2271-2276, 2015.
17. Yue B, Ren QX, Su T, Wang LN and Zhang L: ERK5 silencing inhibits invasion of human osteosarcoma cell via modulating the Slug/MMP-9 pathway. Eur Rev Med Pharmacol Sci 18: 2640-2647, 2014.
18. Yang J, Hou Y, Zhou M, Wen S, Zhou J, Xu L, Tang X, Du YE, Hu P and Liu M: Twist induces epithelial-mesenchymal transition and cell motility in breast cancer via ITGB1-FAK/ILK signaling axis and its associated downstream network. Int J Biochem Cell Biol 71: 62-71, 2016.
19. Livak KJ and Schmittgen TD: Analysis of relative gene expression data using real-time quantitative PCR and the 2(-Delta Delta C(T)) method. Methods 25: 402-408, 2001.
20. Li ZH, Zhou Y, Ding YX, Guo QL and Zhao L: Roles of integrin in tumor development and the target inhibitors. Chin J Nat Med 17: 241-251, 2019.
21. Menakongka A and Suthiphongchai T: Involvement of PI3K and ERK1/2 pathways in hepatocyte growth factor-induced cholangiocarcinoma cell invasion. World J Gastroenterol 16: 713-722, 2010.
22. Sato Y, Harada K, Itatsu K, Ikeda H, Kakuda Y, Shimomura S, Shan Ren X, Yoneda N, Sasaki M and Nakanuma Y: Epithelial-mesenchymal transition induced by transforming growth factor-{beta}1/Snail activation aggravates invasive growth of cholangiocarcinoma. Am J Pathol 177: 141-152, 2010.
23. Techasen A, Namwat N, Loilome W, Bungkanjana P, Khuntikeo N, Puapairoj A, Jearanaikoon P, Saya H and Yongvanit P: Tumor necrosis factor-α (TNF-α) stimulates the epithelial-mesenchymal transition regulator Snail in cholangiocarcinoma. Med Oncol 29: 3083-3091, 2012.
24. Vaquero J, Guedj N, Clapéron A, Nguyen Ho-Bouldoires TH, Paradis V and Fouassier L: Epithelial-mesenchymal transition in cholangiocarcinoma: From clinical evidence to regulatory networks. J Hepatol 66: 424-441, 2017.
25. Hu WW, Chen PC, Chen JM, Wu YM, Liu PY, Lu CH, Lin YF, Tang CH and Chao CC: Periostin promotes epithelial-mesenchymal transition via the MAPK/miR-381 axis in lung cancer. Oncotarget 8: 62248-62260, 2017.
26. Ma L, Young J, Prabhala H, Pan E, Mestdagh P, Muth D, Teruya-Feldstein J, Reinhardt F, Onder TT, Valastyan S, *et al*: miR-9, a MYC/MYCN-activated microRNA, regulates E-cadherin and cancer metastasis. Nat Cell Biol 12: 247-256, 2010.
27. van Roy F and Berx G: The cell-cell adhesion molecule E-cadherin. Cell Mol Life Sci 65: 3756-3788, 2008.
28. Ryu HS, Chung JH, Lee K, Shin E, Jing J, Choe G, Kim H, Xu X, Lee HE, Kim DG, *et al*: Overexpression of epithelial-mesenchymal transition-related markers according to cell dedifferentiation: Clinical implications as an independent predictor of poor prognosis in cholangiocarcinoma. Hum Pathol 43: 2360-2370, 2012.
29. Wang J, Zohar R and McCulloch CA: Multiple roles of alpha-smooth muscle actin in mechanotransduction. Exp Cell Res 312: 205-214, 2006.
30. Ivaska J, Pallari HM, Nevo J and Eriksson JE: Novel functions of vimentin in cell adhesion, migration, and signaling. Exp Cell Res 313: 2050-2062, 2007.
31. Leggett SE, Sim JY, Rubins JE, Neronha ZJ, Williams EK and Wong IY: Morphological single cell profiling of the epithelial-mesenchymal transition. Integr Biol 8: 1133-1144, 2016.
32. İnce AT, Yıldız K, Gangarapu V, Kayar Y, Baysal B, Karatepe O, Kemik AS and Şentürk H: Serum and biliary MMP-9 and TIMP-1 concentrations in the diagnosis of cholangiocarcinoma. Int J Clin Exp Med 8: 2734-2740, 2015.
33. Sun Q, Zhao C, Xia L, He Z, Lu Z, Liu C, Jia M, Wang J and Niu J: High expression of matrix metalloproteinase-9 indicates poor prognosis in human hilar cholangiocarcinoma. Int J Clin Exp Pathol 7: 6157-6164, 2014.
34. Thiery JP, Acloque H, Huang RY and Nieto MA: Epithelial-mesenchymal transitions in development and disease. Cell 139: 871-890, 2009.
35. Watanabe A, Suzuki H, Yokobori T, Altan B, Kubo N, Araki K, Wada S, Mochida Y, Sasaki S, Kashiwabara K, *et al*: Forkhead box protein C2 contributes to invasion and metastasis of extrahepatic cholangiocarcinoma, resulting in a poor prognosis. Cancer Sci 104: 1427-1432, 2013.
36. Li Y, Wang W, Wang W, Yang R, Wang T, Su T, Weng D, Tao T, Li W, Ma D and Wang S: Correlation of TWIST2 up-regulation and epithelial-mesenchymal transition during tumorigenesis and progression of cervical carcinoma. Gynecol Oncol 124: 112-118, 2012.
37. Mao Y, Zhang N, Xu J, Ding Z, Zong R and Liu Z: Significance of heterogeneous Twist2 expression in human breast cancers. PLoS One 7: e48178, 2012.
38. Nitta T, Mitsuhashi T, Hatanaka Y, Miyamoto M, Oba K, Tsuchikawa T, Suzuki Y, Hatanaka KC, Hirano S and Matsuno Y: Prognostic significance of epithelial-mesenchymal transition-related markers in extrahepatic cholangiocarcinoma: Comprehensive immunohistochemical study using a tissue microarray. Br J Cancer 111: 1363-1372, 2014.